Biomaterials 134 (2017) 43–50

Contents lists available at ScienceDirect

Biomaterials

journal homepage: www.elsevier.com/locate/biomaterials

A magnetic droplet vaporization approach using perfluorohexane-encapsulated magnetic mesoporous particles for ultrasound imaging and tumor ablation

Zhaogang Teng [a, e, 1], Ronghui Wang [c, 1], Yang Zhou [c], Michael Kolios [d], Yanjie Wang [d], Nan Zhang [c], Zhigang Wang [c], Yuanyi Zheng [a, b, c, *], Guangming Lu [a, e, **]

[a] Department of Medical Imaging, Jinling Hospital, School of Medicine, Nanjing University, Nanjing, 210002 Jiangsu, PR China
[b] Shanghai Jiaotong University Affiliated Sixth People's Hospital, Shanghai 200233, PR China
[c] Second Affiliated Hospital of Chongqing Medical University, Chongqing 400010, PR China
[d] Department of Physics, Ryerson University, Toronto, Ontario M5B 2K3, Canada
[e] State Key Laboratory of Analytical Chemistry for Life Science, School of Chemistry and Chemical Engineering, Nanjing University, Nanjing, 210093 Jiangsu, PR China

ARTICLE INFO

Article history:
Received 21 December 2016
Received in revised form
11 April 2017
Accepted 12 April 2017
Available online 15 April 2017

Keywords:
Magnetic droplet vaporization
Perflurohexane
Magnetic mesoporous materials
Ultrasound imaging
Tumor ablation

ABSTRACT

Phase change agents consisting of low boiling point perfluorocarbon (PFC) compounds have attracted increasing attention for ultrasound contrast-enhanced imaging and tumor therapy. However, the refraction, acoustic shadowing, reverberation, or limited penetration depth hamper their practical applications through previously reported acoustic droplet vaporization (ADV) or optical droplet vaporization (ODV) technique. Herein, we demonstrate a magnetic droplet vaporization (MDV) approach by loading perflurohexane (PFH) in magnetic mesoporous particles with a hollow space to carry out ultrasound imaging and tumor ablation. *In vitro* and *in vivo* magnetic thermal effects show that magnetic energy can be efficiently transformed into thermal energy by the PFH-encapsulated magnetic mesoporous particles, and then leading to vaporization of the loaded PFH. Owing to the generation of the PFH gas bubbles, the ultrasound signals are greatly improved in both harmonic mode and B mode. Simultaneously, anti-cancer experiments demonstrate that the tumor can be ablated after treating with the MDV method for 4 days, demonstrating highly efficient anti-cancer effects.

1. Introduction

Ultrasound imaging is a widely used and cost-effective clinical diagnostic modality. Ultrasound contrast agents consisting of gas microbubbles can provide a significant acoustic impedance mismatch with aqueous media and oscillate in response to ultrasound pulses to generate non-linear signals, and thus allow to get high quality image, early screen of severe pathologies, and detect the molecular markers on the vascular endothelium and other intravascular targets [1–3]. However, the micrometer sized gas bubbles cannot infiltrate the normal endothelial cells gap or the leaky tumor vasculature with pore size of less than 700 nm, which limits their applications in extravascular imaging [2,4–6]. Recently, phase change contrast agents consisting of low boiling point perfluorocarbon (PFC) compounds have attracted more and more attention because of their vessel penetrated nanometer size and the capability to generate gas bubbles and radiation force under external trigger [7–10]. Owing to the unique properties, phase change contrast agents are appealing for cancer imaging and therapy, such as extravascular ultrasound imaging [11], and enhancement of high intensity focused ultrasound (HIFU) treatment [12,13]. Previously, vaporization of the PFC liquid was realized by using a technique called acoustic droplet vaporization (ADV) [8,13–16], in which the cavitation effect of ultrasound pressure waves induces the liquid nanodroplets to form gas bubbles. However, refraction, acoustic shadowing, and reverberation exist while

* Corresponding author. Department of Medical Imaging, Jinling Hospital, School of Medicine, Nanjing University, Nanjing, 210002 Jiangsu, PR China.
** Corresponding author. Department of Medical Imaging, Jinling Hospital, School of Medicine, Nanjing University, Nanjing, 210002 Jiangsu, PR China.
E-mail addresses: zhengyuanyi@gmail.com (Y. Zheng), cjr.luguangming@vip.163.com (G. Lu).
[1] Z. Teng and R. Wang contributed equally to this work.

http://dx.doi.org/10.1016/j.biomaterials.2017.04.021
0142-9612/

ADV is carried out by using ultrasound. Hence, ADV meets great challenges when it is applied to lesions hidden behind gas-bearing bowel or bones, such as a liver lesion adjacent to a rib. Alternatively, a method termed optical droplet vaporization (ODV) was developed to trigger the vaporization of PFC by using laser irradiation [7,17,18]. However, the interferences of photons with tissues and surrounding media lead to limited penetration depth of only a few centimeters and hamper their effectiveness in theranostics [19–21]. Therefore, it is highly desirable to develop PFC vaporization method with excellent penetration for tumor imaging and therapy.

The tissue penetration of electromagnetic energy is almost not limited. Theoretically, at 500 kHz for example, 99% of energy can penetrate into 15 cm of tissue and be transferred to thermal energy by magnetic nanoparticles [22,23]. This thermal energy generation technique *via* magnetic particle mediators has been used to release drugs with controlled manner [24], remotely regulate protein production *in vivo* [25], and control temperature-sensitive ion channels [26]. In addition, the heat converted by magnetic materials also has been explored to kill cancer cells [27–29]. These unique properties and exciting applications of the magnetic nanoparticles inspire us to develop magnetic droplet vaporization (MDV) approach to vaporize phase change contrast agents for ultrasound imaging and thermal treatment of cancer.

In order to realize the idea of MDV, the compound PFC should be loaded into magnetic materials. However, previously reported phase change contrast agents are generally prepared by encapsulating PFC droplets within lipid, surfactant, or amphiphilic copolymer shells [13,30–32]. The relatively low strength, low heat-resistance, and broad size distribution of the organic molecule stabilized PFC droplets hamper their circulation and acoustic contrast properties. Moreover, they cannot provide magnetic thermal transfer capability for the proposed MDV approach. Recently, hollow mesoporous silica has been subjected to extensive research on nanooncology because of their unique characteristics such as high surface area, uniform pore size, large void space, and good biocompatibility [12,33–40]. Furthermore, their interior spaces can be further functionalized through encapsulating magnetic particles, *viz*, creating magnetic particles embedded hollow mesoporous silica [37,41–43]. The composite particles possess not only large void spaces and permeable outer mesoporous shells but also unique magnetic properties, thus making them ideal candidates to load PFC liquid and then vaporize it upon exposure to an external alternating current (a.c.) magnetic field.

Herein, we introduce the MDV approach by loading perflurohexane (PFH), a highly biocompatible PFC compound with an appropriate phase transition temperature of 56 °C, in magnetic mesoporous particles with a hollow space (denoted as MPs) for the first time to carry out ultrasound imaging and tumor ablation. The PFH-encapsulated MPs (denoted as MDs) successfully integrate the merits of structural stability, accessible mesochannels, excellent magnetic heating capability, and temperature-sensitive property of PFH in one. After exposing to an a.c. magnetic field, the electromagnetic energy can be transformed into thermal energy by the MDs, and PFH are vaporized to form bubbles for enhanced ultrasound imaging. Simultaneously, magnetic thermal produced by the MDs can be used for tumor ablation through the proposed MDV approach.

2. Materials and methods

2.1. Materials

TEOS, cetyltrimethylammonium bromide (CTAB), concentrated ammonia aqueous solution (25 wt%), and anhydrous ethanol were bought from Sinopharm Chemical Reagent Co., Ltd. (Shanghai, China). Perfluorohexane (PFH) was purchased from Sigma-Aldrich Co. LLC (Germany). Millipore water with a resistivity of 18.2 MΩ cm was used in all experiments. RPMI 1640 medium, heat-inactivated fetal bovine serum (FBS), and penicillin-streptomycin solution were purchased from Gibco Laboratories (Invitrogen Co, Grand Island, NY, USA). Cell counting kit-8 (CCK-8) was purchased from Nanjing Keygen Biotech. Co., Ltd. (Nanjing, China). The human embryo kidney 293T cell line and MDA-MB-231 breast cancer cell line were obtained from American Type Culture Collection (ATCC).

2.2. Preparation of perfluorohexane-encapsulated magnetic droplets

The MPs were first prepared according to previously reported method [37]. First, superparamagnetic Fe_3O_4 particles composed of plentiful nanocrystals were prepared *via* a solvothermal approach by using citrate groups as stabilizer [44]. In brief, $FeCl_3$ (0.65 g), trisodium citrate dehydrate (0.20 g), and sodium acetate (1.20 g) were dissolved in ethylene glycol (20 mL) under magnetic stirring. The obtained homogeneous mixture was transferred to a Teflon-lined stainless-steel autoclave with a capacity of 50 mL. The autoclave was heated in an air flow electric oven at 200 °C for 10 h. After cooling down to room temperature, the obtained Fe_3O_4 particles were washed with water for ten times, and dried in vacuum at 60 °C for 12 h. The superparamagnetic Fe_3O_4 particles with citrate groups are highly re-dispersible and can be easily coated with silica through a sol-gel process [45]. Thus, 0.16 g of the Fe_3O_4 particles were dispersed in a mixture of ethanol (100 mL), deionized water (2.0 mL), and concentrated aqueous ammonia solution (3.4 mL, 25 wt%). After adding 280 μL of TEOS and stirring at 40 °C for 24 h, nonporous amorphous silica coated Fe_3O_4 nanoparticles (Fe_3O_4@nSiO_2) were obtained and washed five times with water. The prepared Fe_3O_4@nSiO_2 spheres were re-dispersed in a mixed solution containing CTAB (0.32 g), deionized water (110 mL), ethanol (60 mL), and concentrated aqueous ammonia solution (2.0 mL, 25 wt%). After adding 2.0 mL of TEOS and stirring at 35 °C for 24 h, the product was collected and washed five times with water. Then, the products were incubated in water (160 mL) at 70 °C for 12 h. To remove the CTAB templates, the as-synthesized materials were extracted three times in an ethanol solution (240 mL) containing concentrated HCl (480 μL, 37%) at 60 °C for 3 h. The template-removed MPs were washed with ethanol three times and dried under vacuum. The MPs were weighed (40 mg) and transferred into a 2 mL vials. Then, the vials were capped under vacuum and 1 mL of PFH was added into the vials and placed under 4 °C for another 24 h. Finally, these vials were sonicated in cleaning bath at 4 °C for 1 min after injection of 1 mL saline into the vials and MDs dispersed in 1 mL of saline were obtained.

2.3. Characterization

Transmission electron microscopy (TEM) images were taken using an HT7700 microscope (Hitachi, Tokyo, Japan) operated at an accelerating voltage of 100 kV. The samples were dispersed by ultrasonic in ethanol and dropped on a carbon-coated copper grid for TEM observation. Nitrogen sorption isotherms were measured using a Micromeritics Tristar 3000 analyzer at −196 °C. The samples were degassed at 180 °C for 6 h before the measurements. The Brunauer–Emmett–Teller (BET) method was utilized to calculate the specific surface area (S_{BET}) using the adsorption data at p/p_0 = 0.05–0.15. Pore size analysis was performed by Barrett–Joyner–Halenda (BJH) method from the adsorption branch of isotherm. The total pore volume (V_{total}) was estimated from the adsorbed amount at p/p_0 = 0.995. X-ray diffraction (XRD) pattern

was obtained with a Bruker model D8 focus diffractometer with Cu Kα radiation (0.154 nm) operated at 40 kV and 40 mA. The magnetic characteristics of the magnetic mesoporous particles were measured by a Quantum Design MPMS-XL SQUID magnetometer. The vaporization of the magnetic droplets was observed by an IX71 microscopy (Olympus, Tokyo, Japan). An acoustic microscope (SASAM, Kibero GmbH, Germany) was also used for the vaporization observation. Typically, A drop of MDs dispersed in water was loaded on top of a glass cover slip on the sample stage. Each particle was centered at the foci of the laser and transducer for measurements. A 532 nm laser with a 330 ps pulse width, 4 kHz repetition rate, and a maximum energy of 155 nJ per pulse was focused to a 10 μm spot. The homemade transducer used for this study has a central frequency of 375 MHz. The vaporization process was measured while the laser energy was applied. The temperatures of the samples and tumors were recorded by an infrared camera (Fluke Ti32, Fluke Company, USA). The ultrasound imaging was captured by an ultrasound machine (Mylab90, Esaote Company, Italian).

2.4. Cell viability assay

Human embryo kidney 293T cells were routinely grown in 75 cm^2 plastic culture flasks in RPMI 1640 medium supplemented with 10% (v/v) FBS and 1% (v/v) penicillin-streptomycin solution. The cell viability test was performed using cell counting kit-8 (CCK-8). In brief, the cells were seeded into 96-well cell-culture plate at a density of 1×10^4 cells/well. After growing for 24 h, RPMI 1640 medium containing different concentrations of MDs were added to the cell culture and the cells were grown for an additional 24 h. After adding 10 μL of CCK-8 solution to the culture and incubating for 5 h, the absorbance (A) was measured using an automated microplate reader (BioTek) at the wavelength of 450 nm. The viability of cell growth was calculated by using the following formula: Viability (%) = (mean of absorbance value of treatment group/mean absorbance value of control) × 100. Five duplicate wells were set up for each group and the results were expressed as an average over three nominally identical measurement.

2.5. In vitro magnetic heating and ultrasound imaging

Eppendorf vials containing saline, PFH, and MDs dispersed in saline with concentrations of 5, 10, 20, and 40 mg mL^{-1} were exposed to an a.c. magnetic field of 668 kHz for 0–10 min. Then, the temperature of the vials were determined by a Fluke Ti32 infrared camera (Fluke Company, USA). Evaluation of the ultrasound contrast behavior of the MDs was carried out using 2 mL vials. Typically, saline, PFH, and MDs with concentrations of 5, 10, 20, and 40 mg mL^{-1} in saline were used to achieve the ultrasound imaging before and after exposing to the magnetic field for 5 min. All the samples were scanned by an ultrasonic diagnostic instrument (Mylab90 Esaote Company, Italian) in conventional B-mode and harmonic mode. The transducer of the ultrasound imaging system was LA523. The frequency of harmonic mode was 4–13 MHz, and the depth was 3.7 cm. The derated pressure was 105 kPa.

2.6. In vivo MR imaging

The mice were anesthetized with 1% pentobarbital sodium and received an intravenous injection of 125 μl of MDs solution (6 mg/ml). MRI was conducted on a 7.0 T MR scanner (BioSpec 70/20USR, Bruker, Germany), using a coronal T_2 weighted sequence (TR = 3000 ms, TE = 45 ms, Section Thickness = 0.3 mm, Matrix Size = 256 × 256, FOV = 30 mm × 35 mm, Flip Angle = 90°). The mice were scanned before and after intravenous injection of the MDs (125 μl, 6 mg/ml) for different times (10, 30, 90, 180, and 360 min).

2.7. In vivo magnetic heating, ultrasound imaging, and tumor ablation

All animal experiments were in agreement with the guidelines of the Institutional Animal Care and Use Committee. The MDA-MB-231 breast cancer cells were routinely grown in RPMI-1640 supplemented with FBS (10%, v/v) and penicillin-streptomycin solution (1%, v/v). Then, a suspension of 1×10^6 MDA-MB-231 cells in RPMI-1640 medium without serum (50 μL) was subcutaneously inoculated into 70 BALB/c female nude mice (5 weeks old, 19–20 g). When the tumor volume was approximately 0.7–0.8 cm^3, 400 μL of either saline (n = 5), PFH (n = 5), MPs (40 mg mL^{-1}, n = 5), or MDs (40 mg mL^{-1}, n = 5) were intratumorally injected. The exact amount within the tumor and the amount extravasated was not quantified. After exposing to an a.c. magnetic field of 668 kHz, the temperature of the tumor region was determined by a Fluke Ti32 infrared camera (Fluke Company, USA). Simultaneously, ultrasound imaging of the tumors was also achieved before and after exposing to the a.c. magnetic field.

The therapy ability of the MPs and MDs was further investigated in the mouse breast cancer model. Typically, mice (n = 10) injected with 400 μL of saline, MPs (40 mg mL^{-1}) or MDs (40 mg mL^{-1}) were placed in the center of a magnetic induction coil with a diameter of 3 cm. The exact amount within the tumor and the amount extravasated was not quantified. The exposure to the a.c. magnetic field was started approximately 6 min after injection. The exposure lasted for 6 min and simultaneously temperatures at the tumor region were measured. Following treatment, 5 tumor burden mice was monitored for up to two weeks. The tumor size was calculated as $\pi/6 \times L \times W \times H$. The harvested tumors of other 5 mice and 5 untreated mice were embedded in paraffin, sectioned, and carried out TdT-mediated dUTP nick end labeling (TUNEL) and hematoxylin and eosin staining (H&E). The histological sections were observed under an optical microscope (IX71; Olympus, Tokyo, Japan).

3. Results and discussion

The fabrication process of the MDs is shown in Fig. 1. First, the MPs are prepared *via* a surfactant-assembly sol–gel coating process and a following spontaneous self-transformation procedure. Then, the PFH is infused into the MPs by capillary action. Upon exposing to an a.c. magnetic field, the magnetic energy is efficiently transformed into thermal energy by the magnetic droplets, and thus leading to the vaporization of the loaded PFH to form large number of bubbles. The generated gas bubbles can increase echogenicity for ultrasound imaging, and might be able to enhance the magnetic thermal tumor ablation through streaming and shear induced damage [12].

TEM image clearly shows that the MPs possess a dark magnetic core, a gray silica layer, and a large hollow space between the core and the shell (Fig. 2a), which allow to store large quantities of PFH molecules. The diameter, core size, and shell thickness are measured to be around 585, 310, and 50 nm, respectively. High-magnification TEM images show the shell of the MPs possesses radially oriented mesochannels with openings at surfaces (Fig. S1), meaning that the mesochannels of the particles are readily accessible. Nitrogen sorption isotherms of the MPs show a type IV curve according to the IUPAC nomenclature with a hysteresis loop in the p/p_0 range of 0.4–1.0 (Fig. 2b), revealing characteristics of mesoporous materials. The surface area and pore volume are calculated to be as high as about 550 $m^2\ g^{-1}$ and 0.47 $cm^3\ g^{-1}$, respectively.

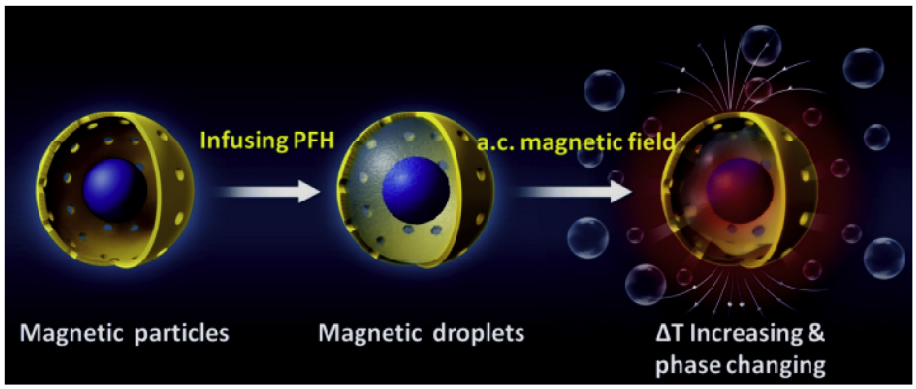

Fig. 1. Schematic illustration of the fabrication process of the magnetic droplets and the mechanism of the magnetic droplets vaporization under an a.c. magnetic field.

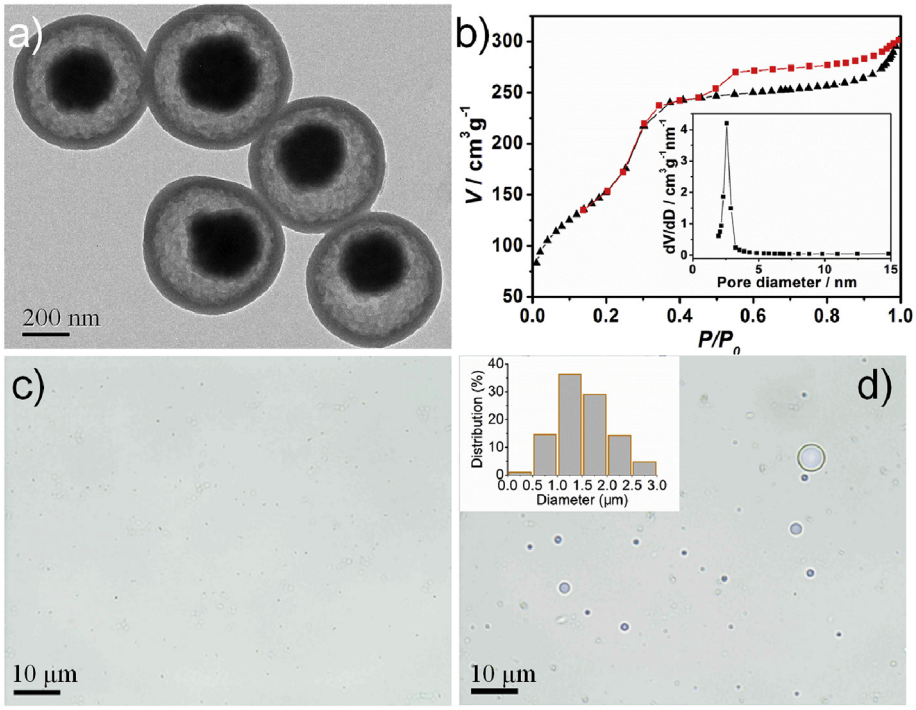

Fig. 2. a) TEM image of the MPs prepared by a surfactant-assembly sol–gel coating process and a following spontaneous self-transformation procedure. b) Nitrogen sorption isotherms and corresponding pore size distribution curve (inset) of the MPs. Optical microscopy images of the MDs before (c) and after (d) exposing to an a.c. magnetic field for 3 min. Inset in (d) is the size distribution of the generated bubbles.

The detailed pore size distribution calculated based on the BJH method reveals the MPs have uniform mesopores of 2.6 nm (Inset in Fig. 2b). The XRD pattern of the MPs shows broad diffraction peaks of magnetite (Fig. S2), suggesting the nanocrystalline structure of the magnetite cores. Magnetic characterization using a magnetometer at 298 K indicates that the MPs have a magnetization saturation value of 29 emu g^{-1} and superparamagnetic character (Fig. S3), which endow the particles with excellent magnetic thermal conversion capability for PFH vaporization and thermal ablation by applying an external a.c. magnetic field. The vaporization ability of the perflurohexane-encapsulated magnetic mesoporous particles was confirmed by optical imaging (Fig. 2c and d). It is clearly observed that large gas bubbles with diameters of 0.5–2.5 μm are presented after exposing the MDs (40 mg mL^{-1}) to an a.c. magnetic field for 3 min (Fig. 2d). Besides, the generation of the PFH gas bubbles was also confirmed by irradiation of 155 nJ pulsed laser on the MDs (Video S1). These results provide direct evidence of the MDV approach.

Supplementary video related to this article can be found at http://dx.doi.org/10.1016/j.biomaterials.2017.04.021

To validate the heating capability of the MDs, saline, PFH, and the MDs dispersed in 1 mL of saline were exposed to an external a.c. magnetic field. The infrared thermal images show that no obvious temperature increasing is observed in the saline and PFH under the a.c. magnetic field (Fig. 3a). In strong contrast, the temperature of the MD solutions increase rapidly after exposing to the a.c. magnetic field. Heat curves show that the solution temperature reaches to 58 °C within 10 min at the MD concentration of 5 mg mL^{-1}, suggesting their strong magnetic thermal transfer capability (Fig. 3b). Moreover, it is observed that the temperature of the MD solutions with concentrations of 5, 10, 20, and 40 mg mL^{-1} increases to 33, 47, 60, and 77 °C upon the a.c. magnetic field for 2 min, indicating that the magnetic heating effect of the MDs is concentration-dependent and the temperature can be easily

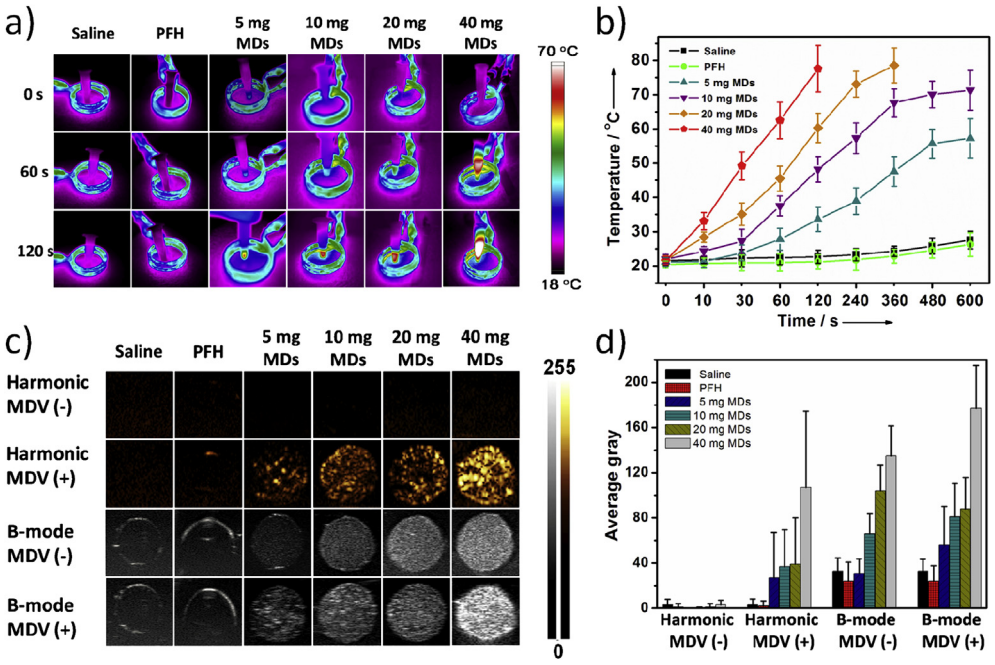

Fig. 3. a) Infrared thermal images and (b) heating curves of eppendorf vials containing saline, PFH, and MDs dispersed in saline with different concentrations after exposing to an a.c. magnetic field of 668 kHz c) *In vitro* ultrasound imaging and corresponding d) gray value of saline, PFH, and MDs with different concentrations under harmonic and conventional B-mode before and after exposing to the a.c. magnetic field for 5 min.

controlled by adjusting the concentration of MDs. Thus, the controllable superior magnetic heating capability not only can be used to vaporize the loaded PFH but also to tumor ablation. Then, the ultrasound imaging performance of the MDs was investigated in harmonic mode and conventional B-mode. As expected, there was almost no ultrasound signal observed in the harmonic mode and conventional B-mode when saline and PFH were used as control (Fig. 3c and d). Also, the signals were very weak for the MD solutions in harmonic mode without magnetic heating. In contrast, it is obviously observed that the ultrasound signals are greatly enhanced and increased with the concentration of MDs after exposing to the a.c. magnetic field. The improvement of ultrasound imaging through an external magnetic field is also observed in the conventional B-mode. These results further indicate that PFH gas bubbles are generated *via* the MDV approach and lead to strong echoes for ultrasound imaging.

The *in vitro* biocompatibility of the MDs was studied prior to biological experiments by a typical CCK-8 assay (Fig. S4). It was observed that the cell viability retained 80% even when they were incubated with the MDs at a concentration of as high as 400 μg mL^{-1} for 24 h, indicating good biocompatibility of the MDs. In order to demonstrate the utility of this MDs, we examined the *in vivo* magnetic thermal effect and ultrasound imaging performance of the MDs upon an a.c. magnetic field. After intratumoral injection of 0.4 mL of saline, PFH, MPs (40 mg mL^{-1}), and MDs (40 mg mL^{-1}), the mice were placed in a water-cooled magnetic induction coil with a diameter of 3 cm and exposed to a.c. magnetic field (Fig. S5). The surface temperatures of the tumor injected with MPs and MDs gradually increase to 55 °C and 57 °C after 3 min (Fig. 4a and b). In comparison, the tumor temperatures on mice injected with saline and PFH under the same a.c. magnetic field show little changes. Simultaneously, the infrared imaging show that the domains heated by the MDs are obviously large than those by the MPs (Fig. 4a), which is attributed to the fast heat transport in tumor induced by the vaporized PFH (boiling point 56 °C). These results suggest the temperature of tumor can be effectively controlled by the MDV approach. Furthermore, the MDV approach for the enhancement of ultrasound imaging is investigated *in vivo* under harmonic mode and B-mode. The imaging results show that only very weak ultrasonic echoes could be detected in the harmonic mode when saline, PFH, or MPs control are injected (Fig. 4c and d). In contrast, the strong ultrasound signal can be observed at the tumor after injecting the MDs and exposing to the a.c. magnetic field. The gray value at the tumor is measured up to 135 through the MDV approach. However, the values before and after injection of the MDs are only 4 and 30. The enhancement of ultrasound imaging by the MDV approach also observed in the B-mode. These results demonstrate that MDs can offer significantly enhanced ultrasound imaging contrast under an a.c. magnetic field, which endows them with great potential in ultrasound imaging and simultaneous ultrasound-guided cancer therapy. In addition, owing to the encapsulation of superparamagnetic Fe_3O_4 cores, the MDs display excellent T_2-weighted MRI capability (Figs. S6 and S7), thus the MDs also provide a strategy for ultrasound and magnetic resonance dual-modality imaging.

The therapy ability of the MDs was further investigated in tumor bearing mouse model. The mouse was placed in a magnetic induction coil and exposed to an a.c. magnetic field for 6 min. Following treatment, the tumor burden was monitored for up to two weeks. Apparent anti-cancer effects in MPs and MDs treated group were observed two weeks post-therapy (Fig. 5a and b). Compared with the saline group, the relative tumor volume was significantly reduced after the treatment with the MPs and MDs for 4 days, suggesting the intratumoral fractions of MPs and MDs was sufficient to shrink the tumor. Hematoxylin and eosin (H&E) staining and TdT-mediated dUTP nick end labeling (TUNEL) of the tumor sections were also carried out after the treatment for 1 day. The results show the structure of tumor cells is intact and no apparent cell apoptosis is noticed in the saline group (Fig. 6a and d). In contrast, large necrotic regions with coagulated cell nuclei and disappeared cell structure are presented in the tumor after treatment with the MPs and MDs (Fig. 6b and c). TUNEL staining shows

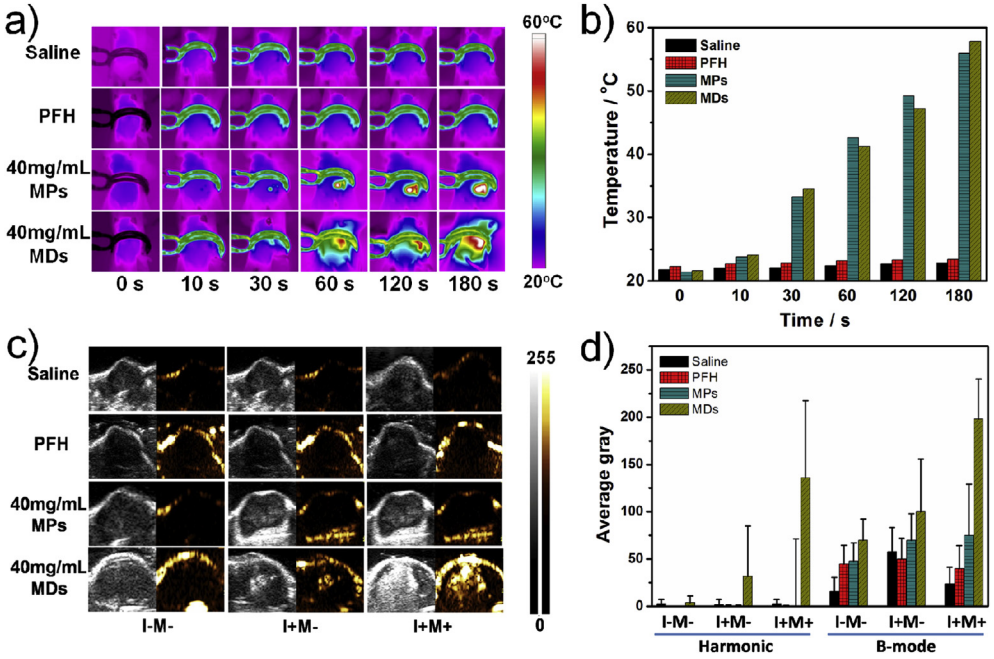

Fig. 4. a) Infrared thermal images and (b) temperature of tumor-bearing mice (n = 5) with saline, PFH, MPs, and MDs injection exposed to a.c. magnetic field of 668 kHz for different time. c) *In vivo* ultrasound imaging and (d) corresponding gray values of tumor injected with saline, PFH, MPs, and MDs under conventional B-mode (left panel) and harmonic mode (right panel) before and after exposing to the a.c. magnetic field of. I and M represent the injection and a.c. magnetic field, respectively.

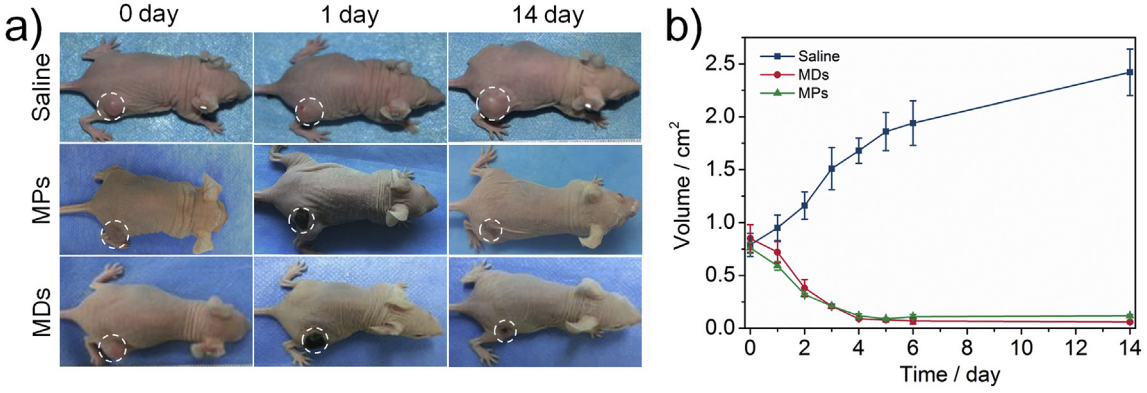

Fig. 5. a) Representative photos and (b) tumor growth curves of tumor-bearing mice (n = 10) injected with saline MPs, and MDs and exposed to an a.c. magnetic field of 668 kHz for 6 min. Tumor volumes were normalized to their initial sizes.

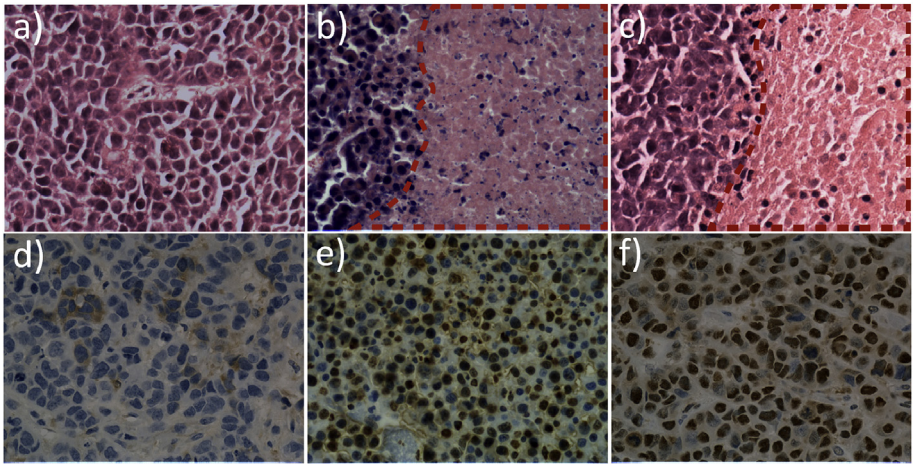

Fig. 6. (a, b, c) H&E stain and (d, e, f) TUNEL stain of tumors exposed to an a.c. magnetic field of 668 kHz after injecting with (a, d) saline, (b, e) MPs, and (c, f) MDs. The images shown here are 400× magnification.

that numerous tumor cells are brown, further indicates the apoptosis of the tumor cells (Fig. 6e and f). Furthermore, we injected the magnetic droplets intravenously into 6 week nude mice without tumor and acquired MR imaging. It is observed the T_2-weight MR signal of the liver is gradually decreased after injection of the magnetic droplets (Figs. S8 and S9). These results suggest that the magnetic droplets are injectable.

4. Conclusions

In summary, we proposed a MDV approach by using PFH-encapsulated magnetic mesoporous particles to carry out ultrasound imaging and tumor ablation. The PFH-encapsulated MDs possess accessible mesochannels, excellent magnetic heating capability, and temperature-sensitive property of PFH. After exposing to an a.c. magnetic field of 668 kHz for 2 min, the temperature of the MD solutions can controllably and efficiently heated up to 77 °C, and leading to the vaporization of the loaded PFH. Owing to the generation of the PFH gas bubbles, the phantom and animal studies show that ultrasound signals are greatly improved in both harmonic mode and conventional B-mode. *In vivo* magnetic thermal effect shows that the tumor region can be rapidly heated to 57 °C by using the MDs. Anti-cancer experiments demonstrate that MPs and MDs cause tumor regression.

Acknowledgment

We greatly appreciate financial support from the National Key Basic Research Program of the PRC (2014CB744504 and 2014CB744501), the Major International (Regional) Joint Research Program of China (81120108013), the National Natural Science Foundation of China (81425014, 30930028, 81201175, 21603106, and 81227801), the Chongqing Distinguished Young Scholars Foundation (cstc2013jcyjjq10004), and the Natural Science Foundation of Jiangsu Province (BK20160017).

Appendix A. Supplementary data

Supplementary data related to this article can be found at http://dx.doi.org/10.1016/j.biomaterials.2017.04.021.

References

[1] J.R. Lindner, Molecular imaging of cardiovascular disease with contrast-enhanced ultrasonography, Nat. Rev. Cardiol. 6 (2009) 475–481.
[2] S. Son, H.S. Min, D.G. You, B.S. Kim, I.C. Kwon, Echogenic nanoparticles for ultrasound technologies: evolution from diagnostic imaging modality to multimodal theranostic agent, Nano Today 9 (2014) 525–540.
[3] H. Ke, J. Wang, Z. Dai, Y. Jin, E. Qu, Z. Xing, C. Guo, X. Yue, J. Liu, Gold-nanoshelled microcapsules: a theranostic agent for ultrasound contrast imaging and photothermal therapy, Angew. Chem. Int. Ed. 50 (2011) 3017–3021.
[4] M.G. Shapiro, P.W. Goodwill, A. Neogy, M. Yin, F.S. Foster, D.V. Schaffer, S.M. Conolly, Biogenic gas nanostructures as ultrasonic molecular reporters, Nat. Nanotechnol. 9 (2014) 311–316.
[5] Y. Chen, Y. Gao, H. Chen, D. Zeng, Y. Li, Y. Zheng, F. Li, X. Ji, X. Wang, F. Chen, Q. He, L. Zhang, J. Shi, Engineering inorganic nanoemulsions/nanoliposomes by fluoride-silica chemistry for efficient delivery/co-delivery of hydrophobic agents, Adv. Funct. Mater 22 (2012) 1586–1597.
[6] Z. Zha, J. Wang, E. Qu, S. Zhang, Y. Jin, S. Wang, Z. Dai, Polypyrrole hollow microspheres as echogenic photothermal agent for ultrasound imaging guided tumor ablation, Sci. Rep. 3 (2013) 2–8.
[7] K. Wilson, K. Homan, S. Emelianov, Biomedical photoacoustics beyond thermal expansion using triggered nanodroplet vaporization for contrast-enhanced imaging, Nat. Commun. 3 (2012) 618–627.
[8] D. Kagan, M.J. Benchimol, J.C. Claussen, E. Chuluun-Erdene, S. Esener, J. Wang, Acoustic droplet vaporization and propulsion of perfluorocarbon-loaded microbullets for targeted tissue penetration and deformation, Angew. Chem. Int. Ed. 51 (2012) 7519–7522.
[9] P.S. Sheeran, S.H. Luois, L.B. Mullin, T.O. Matsunaga, P.A. Dayton, Design of ultrasonically-activatable nanoparticles using low boiling point perfluorocarbons, Biomaterials 33 (2012) 3262–3269.
[10] W. Cai, X. Chen, Nanoplatforms for targeted molecular imaging in living subjects, Small 3 (2007) 1840–1854.
[11] T.O. Matsunaga, Phase-change nanoparticles using highly volatile perfluorocarbons: toward a platform for extravascular ultrasound imaging, Theranostics 2 (2012) 1185–1198.
[12] X. Wang, H. Chen, Y. Chen, M. Ma, K. Zhang, F. Li, Y. Zheng, D. Zeng, Q. Wang, J. Shi, Perfluorohexane-encapsulated mesoporous silica nanocapsules as enhancement agents for highly efficient high Intensity focused ultrasound (HIFU), Adv. Mater 24 (2012) 785–791.
[13] Y. Zhou, Z. Wang, Y. Chen, H. Shen, Z. Luo, A. Li, Q. Wang, H. Ran, P. Li, W. Song, Z. Yang, H. Chen, Z. Wang, G. Lu, Y. Zheng, Microbubbles from gas-generating perfluorohexane nanoemulsions for targeted temperature-sensitive ultrasonography and synergistic HIFU ablation of tumors, Adv. Mater 25 (2013) 4123–4130.
[14] O.D. Kripfgans, J.B. Fowlkes, D.L. Miller, O.P. Eldevik, P.L. Carson, Acoustic droplet vaporization for therapeutic and diagnostic applications, Ultrasound Med. Biol. 26 (2000) 1177–1189.
[15] C.-Y. Lin, W.G. Pitt, Acoustic droplet vaporization in biology and medicine, Biomed. Res. Int. 2013 (2013) 1–13.
[16] C.-H. Wang, S.-T. Kang, Y.-H. Lee, Y.-L. Luo, Y.-F. Huang, C.-K. Yeh, Aptamer-conjugated and drug-loaded acoustic droplets for ultrasound theranosis, Biomaterials 33 (2012) 1939–1947.
[17] E. Strohm, M. Rui, I. Gorelikov, N. Matsuura, M. Kolios, Vaporization of perfluorocarbon droplets using optical irradiation, Biomed. Opt. Express 2 (2011) 1432–1442.
[18] J. Jian, C. Liu, Y. Gong, L. Su, B. Zhang, Z. Wang, D. wang, Y. Zhou, F. Xu, P. Li, Y. Zheng, L. Song, X. Zhou, India ink incorporated multifunctional phase-transition nanodroplets for photoacoustic/ultrasound dual-modality imaging and photoacoustic effect based tumor therapy, Theranostics 4 (2014) 1026–1038.
[19] A.M. Smith, M.C. Mancini, S. Nie, Second window for in vivo imaging, Nat. Nanotechnol. 4 (2009) 710–711.
[20] L. Nie, X. Chen, Structural and functional photoacoustic molecular tomography aided by emerging contrast agents, Chem. Soc. Rev. 43 (2014) 7132–7170.
[21] P. Huang, P. Rong, J. Lin, W. Li, X. Yan, M.G. Zhang, L. Nie, G. Niu, J. Lu, W. Wang, X. Chen, Triphase interface synthesis of plasmonic gold bellflowers as near-infrared light mediated acoustic and thermal theranostics, J. Am. Chem. Soc. 136 (2014) 8307–8313.
[22] A.M. Derfus, G. von Maltzahn, T.J. Harris, T. Duza, K.S. Vecchio, E. Ruoslahti, S.N. Bhatia, Remotely triggered release from magnetic nanoparticles, Adv. Mater 19 (2007) 3932–3936.
[23] J.H. Young, M.T. Wang, I.A. Brezovich, Frequency/depth-penetration considerations in hyperthrmia by magnetically induced currents, Electron. Lett. 16 (1981) 358–359.
[24] C.R. Thomas, D.P. Ferris, J.-H. Lee, E. Choi, M.H. Cho, E.S. Kim, J.F. Stoddart, J.-S. Shin, J. Cheon, J.I. Zink, Noninvasive remote-controlled release of drug molecules in magnetic actuation of mechanized nanoparticles, J. Am. Chem. Soc. 132 (2010) 10623–10625.
[25] S.A. Stanley, J.E. Gagner, S. Damanpour, M. Yoshida, J.S. Dordick, J.M. Friedman, Radio-wave heating of iron oxide nanoparticles can regulate plasma glucose in mice, Science 336 (2012) 604–608.
[26] H. Huang, S. Delikanli, H. Zeng, D.M. Ferkey, A. Pralle, Remote control of ion channels and neurons through magnetic-field heating of nanoparticles, Nat. Nanotechnol. 5 (2010) 602–606.
[27] K.H. Bae, M. Park, M.J. Do, N. Lee, J.H. Ryu, G.W. Kim, C. Kim, T.G. Park, T. Hyeon, Chitosan oligosaccharide-stabilized ferrimagnetic iron oxide nanocubes for magnetically modulated cancer hyperthermia, ACS Nano 6 (2012) 5266–5273.
[28] A. Meffre, B. Mehdaoui, V. Kelsen, P.F. Fazzini, J. Carrey, S. Lachaize, M. Respaud, B. Chaudret, A simple chemical route toward monodisperse iron carbide nanoparticles displaying tunable magnetic and unprecedented hyperthermia properties, Nano Lett. 12 (2012) 4722–4728.
[29] Y. Zhou, R. Wang, Z. Teng, Z. Wang, B. Hu, M. Kolios, H. Chen, N. Zhang, Y. Wang, P. Li, X. Wu, G. Lu, Y. Chen, Y. Zheng, Magnetic nanoparticle-promoted droplet vaporization for in vivo stimuli-responsive cancer theranostics, NPG Asia Mater 8 (2016) e313.
[30] K.W. Ferrara, M.A. Borden, H. Zhang, Lipid-shelled vehicles: engineering for ultrasound molecular imaging and drug delivery, Acc. Chem. Res. 42 (2009) 881–892.
[31] N. Rapoport, K.-H. Nam, R. Gupta, Z. Gao, P. Mohan, A. Payne, N. Todd, X. Liu, T. Kim, J. Shea, C. Scaife, D.L. Parker, E.-K. Jeong, A.M. Kennedy, Ultrasound-mediated tumor imaging and nanotherapy using drug loaded, block copolymer stabilized perfluorocarbon nanoemulsions, J. Control. Release 153 (2011) 4–15.
[32] Z. Xing, J. Wang, H. Ke, B. Zhao, X. Yue, Z. Dai, J. Liu, The fabrication of novel nanobubble ultrasound contrast agent for potential tumor imaging, Nanotechnology 21 (2010) 145607–145615.
[33] Y. Chen, H. Chen, L. Guo, Q. He, F. Chen, J. Zhou, J. Feng, J. Shi, Hollow/rattle-type mesoporous nanostructures by a structural difference-based selective etching strategy, ACS Nano 4 (2010) 529–539.
[34] F. Tang, L. Li, D. Chen, Mesoporous silica nanoparticles: synthesis, biocompatibility and drug delivery, Adv. Mater 24 (2012) 1504–1534.
[35] L. Du, S. Liao, H.A. Khatib, J.F. Stoddart, J.I. Zink, Controlled-access hollow mechanized silica nanocontainers, J. Am. Chem. Soc. 131 (2009)

15136–15142.
[36] Z. Teng, S. Wang, X. Su, G. Chen, Y. Liu, Z. Luo, W. Luo, Y. Tang, H. Ju, D. Zhao, G. Lu, Facile synthesis of yolk-shell structured inorganic-organic hybrid spheres with ordered radial mesochannels, Adv. Mater 26 (2014) 3741–3747.
[37] Z. Teng, X. Su, Y. Zheng, J. Sun, G. Chen, C. Tian, J. Wang, H. Li, Y. Zhao, G. Lu, Mesoporous silica hollow spheres with ordered radial mesochannels by a spontaneous self-transformation approach, Chem. Mater 25 (2013) 98–105.
[38] Y. Fang, G. Zheng, J. Yang, H. Tang, Y. Zhang, B. Kong, Y. Lv, C. Xu, A.M. Asiri, J. Zi, F. Zhang, D. Zhao, Dual-pore mesoporous carbon@silica composite core-shell nanospheres for multidrug delivery, Angew. Chem. Int. Ed. 53 (2014) 5366–5370.
[39] M. Wang, Z. Sun, Q. Yue, J. Yang, X. Wang, Y. Deng, C. Yu, D. Zhao, An interface-directed coassembly approach to synthesize uniform large-pore mesoporous silica spheres, J. Am. Chem. Soc. 136 (2014) 1884–1892.
[40] Z. Teng, X. Su, B. Lee, C. Huang, Y. Liu, S. Wang, J. Wu, P. Xu, J. Sun, D. Shen, W. Li, G. Lu, Yolk–shell structured mesoporous nanoparticles with thioether-bridged organosilica frameworks, Chem. Mater 26 (2014) 5980–5987.
[41] Y. Chen, H. Chen, D. Zeng, Y. Tian, F. Chen, J. Feng, J. Shi, Core/shell structured hollow mesoporous nanocapsules: a potential platform for simultaneous cell imaging and anticancer drug delivery, ACS Nano 4 (2010) 6001–6013.
[42] J. Liu, S.Z. Qiao, S.B. Hartono, G.Q. Lu, Monodisperse yolk-shell nanoparticles with a hierarchical porous structure for delivery vehicles and nanoreactors, Angew. Chem. Int. Ed. 49 (2010) 4981–4985.
[43] Z. Teng, J. Li, F. Yan, R. Zhao, W. Yang, Highly magnetizable superparamagnetic iron oxide nanoparticles embedded mesoporous silica spheres and their application for efficient recovery of DNA from agarose gel, J. Mater. Chem. 19 (2009) 1811–1815.
[44] J. Liu, Z. Sun, Y. Deng, Y. Zou, C. Li, X. Guo, L. Xiong, Y. Gao, F. Li, D. Zhao, Highly water-dispersible biocompatible magnetite particles with low cytotoxicity stabilized by citrate groups, Angew. Chem. Int. Ed. 48 (2009) 5875–5879.
[45] Z. Teng, C. Sun, X. Su, Y. Liu, Y. Tang, Y. Zhao, G. Chen, F. Yan, N. Yang, C. Wang, G. Lu, Superparamagnetic high-magnetization composite spheres with highly aminated ordered mesoporous silica shell for biomedical applications, J. Mater. Chem. B 1 (2013) 4684–4691.